Microrheological characterization of covalent adaptable hydrogel degradation in response to temporal pH changes that mimic the gastrointestinal tract

Nan Wu and Kelly M. Schultz*

Department of Chemical and Biomolecular Engineering, Lehigh University, Bethlehem, PA, 18015

E-mail: kes513@lehigh.edu

Phone: (610) 758-2012. Fax: (610) 758-5057

Supporting Information

Materials

The two polymers that make up our covalent adaptable hydrogel scaffold (CAH) are 8-arm star poly(ethylene glycol) (PEG)-hydrazine (M_n 10 000 g mol^{-1}, $f = 8$, where f is the functionality) and 8-arm star PEG-aldehyde (M_n 10 000 g mol^{-1}, $f = 8$) are synthesized and provided by the Anseth lab (University of Colorado at Boulder). In this work, we use the same batches that are characterized in their previous publications.[1–3] In these publications, the synthesis protocols of the PEG-hydrazine and PEG-aldehyde and the NMR results are included.[2,3] These materials are used as received.

Sample preparation

To enable microrheological measurements, 0.04% solids per volume of 1 μm fluorescently labeled polystyrene carboxylated probe particles ($2a = 1.0 \pm 0.02$ μm, where a is the particle radius, Polysciences Inc.) are added to a polymeric precursor solution that forms the CAH. Prior to adding them to this solution, the fluorescent probe particles are washed 3$\times$ by centrifugation at 5 000 RPM for 5 min (Centrifuge 5424, Eppendorf) and resuspension to remove impurities and excess dye from the probe stock solution. Particles are then sonicated at 40 kHz for 15 min (Emerson Industrial Automation) to remove any probe aggregates and ensure redispersion.

The washed probe particles are added to the precusor solution of 4.4 wt% PEG-aldehyde and 200 mM pH 7.4 HEPES buffer (Fisher BioReagents, Fisher Scientific). The gelation reaction is initiated by mixing this precursor solution with a precursor solution of 4.4 wt% PEG-hydrazine in 1$\times$ PBS buffer. Since gelation occurs rapidly, the mixed solution (10 μL) is quickly injected into the sample chamber of the microfluidic device (10 mm diameter by 1 mm height) prior to gelation. After gelation, the CAH scaffold forms a 3D cross-linked network in the sample chamber and is initially incubated at pH 5.5 in an acetic acid/sodium acetate buffer solution at room temperature.[4] The estimated hydrogel cross-linking efficiency is 41.7%.[2]

Buffer solutions

In these experiments three buffer solutions have been used, pH 4.3, 5.5 and 7.4. Each buffer mimics the pH of different parts of the digestive tract. pH 4.3 buffer consists of 74 mM acetic acid (certified ACS, Fisher Scientific) and 26 mM sodium acetate (anhydrous lab grade, Fisher Scientific). The composition of the pH 5.5 buffer includes 15 mM acetic acid and 85 mM sodium acetate. pH 7.4 buffer is made with 200 mM 4-(2-hydroxyethyl)-1-piperazineethanesulfonic acid (HEPES, Fisher Scientific) and 1 M sodium hydroxide (NaOH, Fisher Scientific). Each buffer pH is adjusted to the desired value by drop-wise addition of

1 M hydrochloric acidic (HCl, Ricca Chemical Company, LLC) or 1 M NaOH.

Methods

Multiple particle tracking microrheology

CAH degradation in pH environments that mimic the GI tract is characterized using multiple particle tracking microrheology (MPT). In all experiments, 1 μm fluorescently labeled carboxylated polystyrene probe particles ($2a = 1.0 \pm 0.02$ μm, Polysciences, Inc.) are used. The negative surface charge and concentration are chosen to ensure that there are no particle-particle and particle-polymer interactions, enabling accurate MPT measurements. MPT data are collected in the center of the sample every $6 - 10$ min throughout degradation. An inverted microscope (Observer Z1, Carl Zeiss AG) with a 63$\times$ water immersion objective with a low numerical aperture (N.A. 1.3, 1$\times$ optovar, Carl Zeiss AG) is used to collect video microscopy for MPT. Videos are recorded using a high-speed camera (Phantom Miro M120, 1024×1024 pixels, Vision Research Inc.) at 30 frames per second for 800 frames with an exposure time of 1000 μs. These settings are chosen to minimize static and dynamic particle tracking errors.[5] Using classic tracking algorithms developed by Crocker and Grier, each particle is tracked by identifying the brightness-weighted centroid of the probe particle using IDL. Then the positions of each particle in each frame are linked into trajectories using a probability distribution function that accounts for the thermal motion of a single particle.[6–10] $50 - 100$ particles are tracked in each video. For all particles, the ensemble-averaged mean-squared displacement (MSD, $\langle \Delta r^2(\tau) \rangle$) is calculated from particle trajectories using the equation $\langle \Delta r^2(\tau) \rangle = \langle \Delta x^2(\tau) \rangle + \langle \Delta y^2(\tau) \rangle$, where τ is the lag time, and x and y are particle positions in the 2D plane.

MSDs for GI tract 1 and 2

Examples of MSDs for experiments in GI tract 1 and 2 are shown in Figure S1 and S2, respectively.

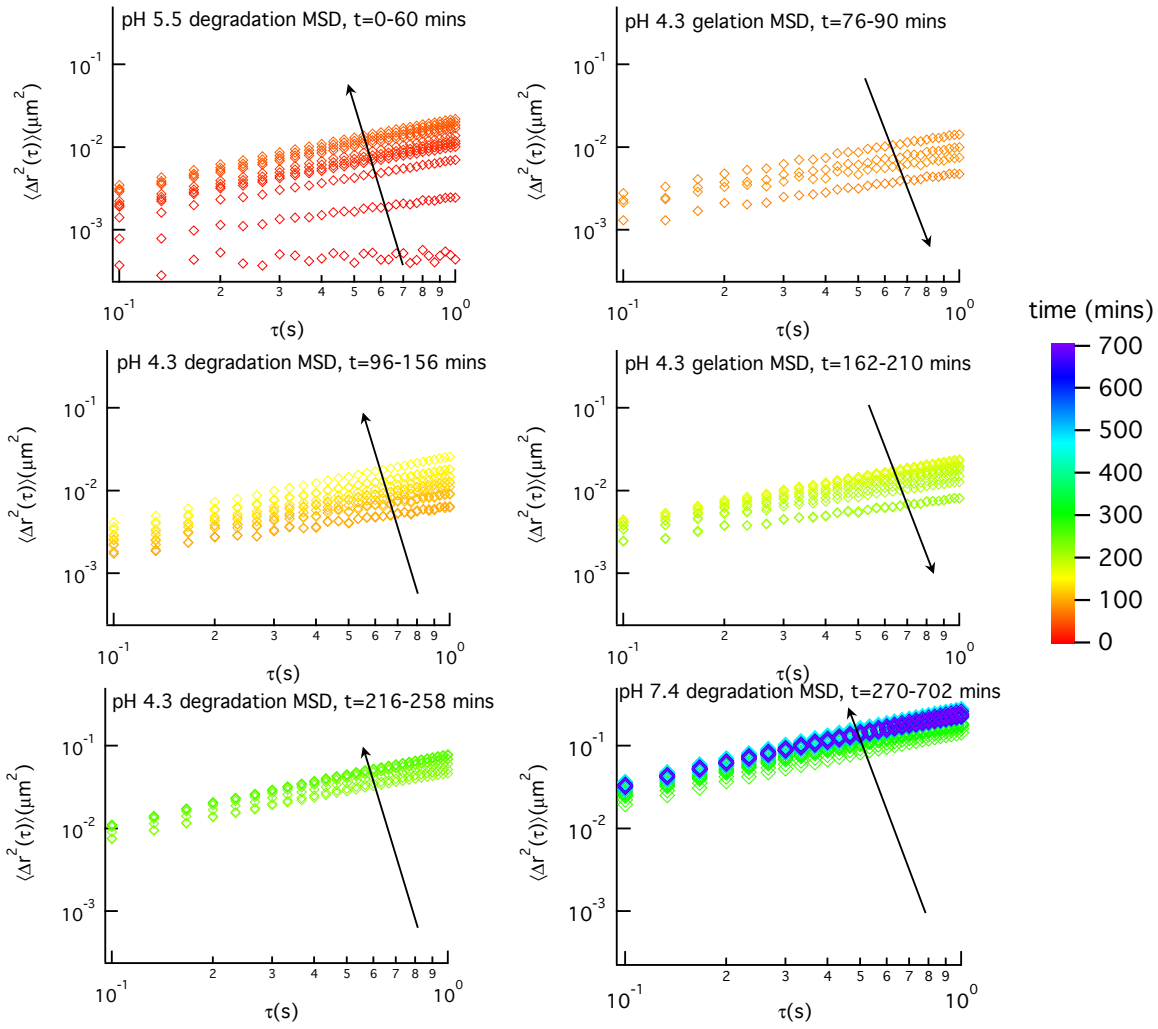

Figure S1: μ^2rheology measurements for CAH degradation in GI tract 1 corresponding to Figure 3a in the manuscript. The temporal pH changes in GI tract 1 are consecutive degradation in pH 5.5, 4.3 and 7.4. The mean-squared displacement (MSD), $\langle \Delta r^2(\tau) \rangle$, is plotted as a function of lag time. The arrows indicate the material evolution either undergoing degradation or gelation over time.

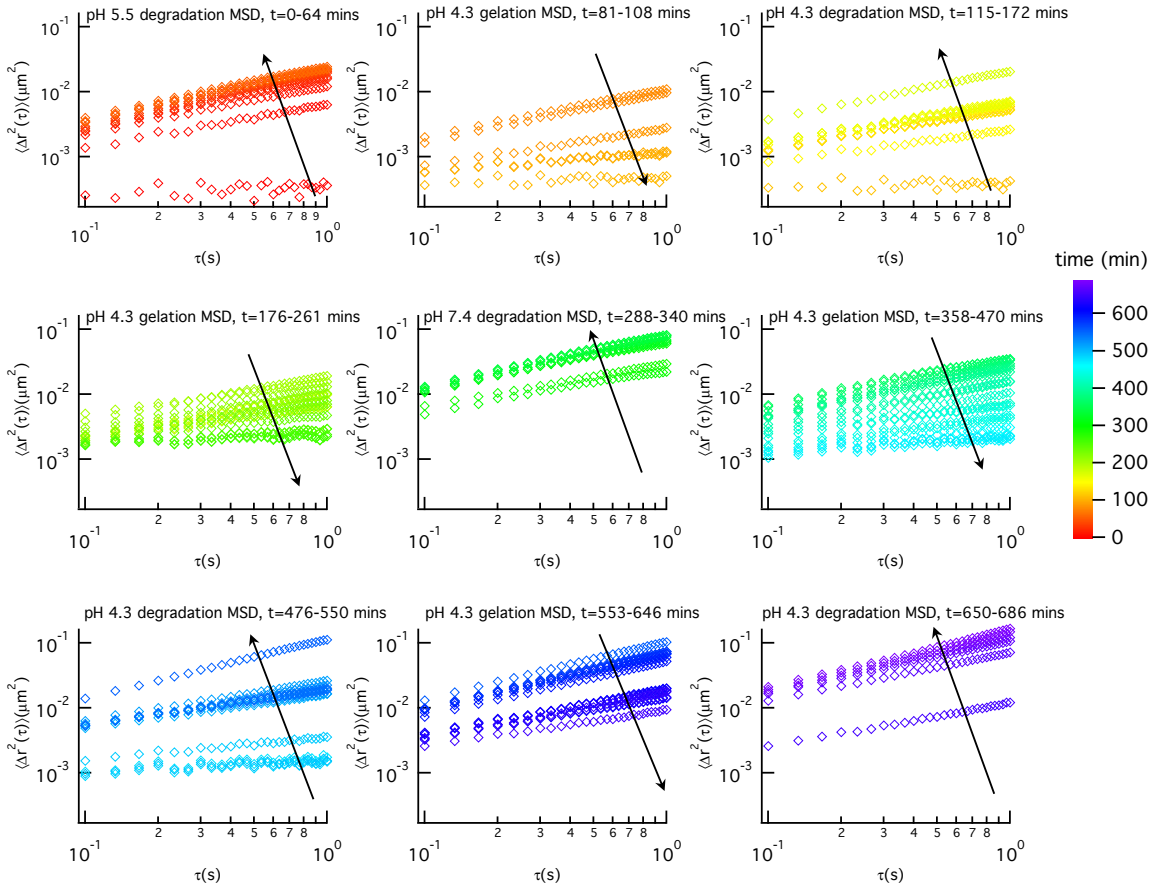

Figure S2: μ^2rheology measurements for CAH degradation in GI tract 2 corresponding to Figure 4 in the manuscript. The temporal pH changes in GI tract 2 are consecutive degradation in pH 5.5, 4.3, 7.4 and 4.3. The mean-squared displacement (MSD), $\langle \Delta r^2(\tau) \rangle$, is plotted as a function of lag time. The arrow indicates the material evolution either undergoing degradation or gelation over time.

Time-cure superposition

The critical relaxation exponent, n, and critical degradation time, t_c, are determined using time-cure superposition (TCS) for CAH degradation at pH 4.3, 5.5 and 7.4.[4] TCS is the superposition of viscoelastic functions at different extents of reaction.[10–18] MSDs measure the longest relaxation time of the polymer in the sol and the network in the gel. Since they measure different relaxation times pre- and post-gelation, the shape of the MSD curves are distinct in the pre- and post-gel. This technique uses the self-similar shape of MSD curves to shift them into a gel and a sol master curve using shift factors a and b. The lag time, τ, is shifted by shift factor a, which relates to the longest relaxation time, τ_L, and the distance away from critical extent of degradation, $\epsilon = \frac{|t-t_c|}{t_c}$, by scaling exponent y, using the relation $a \sim \tau_L^{-1} \sim \epsilon^y$. MSDs are shifted by shift factor b, which relates to the steady state creep compliance, J_e, and the distance away from critical extent of degradation by scaling exponent z, using the relation $b \sim J_e^{-1} \sim \epsilon^z$. The ratio of the scaling exponents is the critical relaxation exponent $n = \frac{z}{y}$.[11–15,17–20] n is also the slope at the intersection of the two master curves and quantitatively identifies the transition from gel to sol. $n_{avg} = 0.79 \pm 0.05$ is the average value of n from MPT measurements of CAH degradation at single pHs. Previous work, characterized CAH degradation at pH 4.3 and 7.4. Additional control experiments at pH 5.5 were done for this work. These experiments measured degradation at pH 4.3, 5.5 and 7.4 and calculated $n = 0.73 \pm 0.08$, $n = 0.85 \pm 0.11$ and $n = 0.79 \pm 0.06$, respectively. Each average value of n is calculated from at least three experiments with the error propagated from these experiments.

An example of each of these single pH experiments is shown in Figure S3. Here the logarithmic slope of the MSD, α, is plotted as a function of time. The dashed lines are the upper and lower limits of the average critical relaxation exponent, which bounds the critical transition region (shaded in gray).

Figure S3a shows material degradation at acidic incubation pH (pH 4.3), where the gel is first fabricated at pH 7.4. The large oscillation, the degradation-gelation cycles, arise due

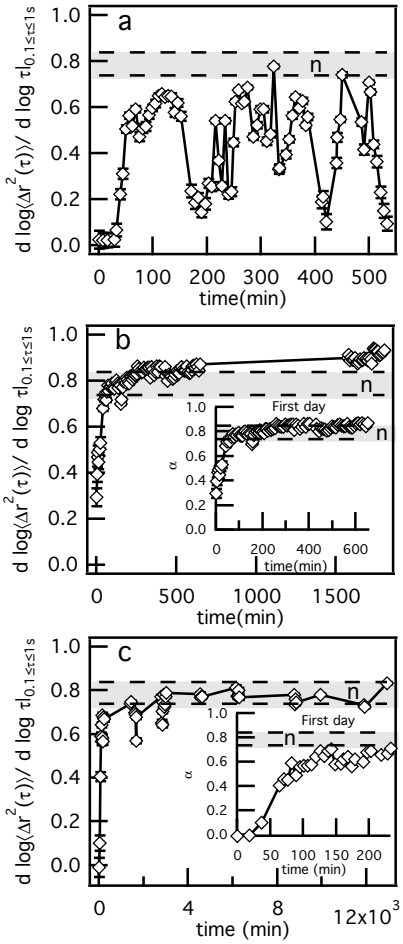

Figure S3: μ^2rheology measurements of CAH degradation at a single pH. The logarithmic slope of the mean-squared displacement (MSD), $\alpha = \frac{d \log \langle \Delta r^2(\tau) \rangle}{d \log \tau}$, as a function of time during degradation. Degradation of the CAH is done at (a) pH 4.3, (b) 5.5 and (c) 7.4. The inset in (b) and (c) is the first day of measurements. The horizontal dashed lines bound the phase transition region identified from calculating the critical relaxation exponent, n. The average value of n for all single pH degradation is $n_{avg} = 0.79 \pm 0.05$ determined using time-cure superposition.

to the change in pH which pushes the hydrazone network bonds out of equilibrium. When incubated at pH 4.3, the equilibrium immediately shifts towards degradation due to bond hydrolysis. As degradation continues a new equilibrium state occurs and the the material shifts to bond formation, which causes the material to re-gel. Previous work derived a kinetic model from MPT data to describe scaffold degradation at different pHs.[16] At pH 4.3, degradation is a 2^{nd}-order reaction, the detailed discussion of this model can be found in Reference 16.

The degradation profile at pH 5.5 is shown in Figure S3b, where the scaffold is made at pH 7.4. This degradation profile is similar to degradation at pH 7.4 (where material is gelled at pH 4.3), shown in Figure S3c. The material has relatively fast initial degradation and after it reaches the gel-sol transition region, the material oscillates around this transition region until complete degradation. At pH 5.5, complete degradation takes two days. At pH 7.4, complete degradation takes at least 10 days. These degradation profiles are also due to the reaction kinetics of hydrazone network bonds at those pHs. The degradation at pH 5.5 and 7.4 are described using a 1^{st}-order kinetic model. As the material is pushed out of equilibrium by incubation in a different pH, the equilibrium shifts strongly towards network bond hydrolysis with little or no bond formation taking place during the initial degradation. Then the reaction shift towards simultaneous bond hydrolysis and reformation, however, polymer has already diffused out of the scaffold during the initial degradation. Therefore, there is less polymer available for network bond reformation, resulting in a smaller extent of bond breakage and reformation until final degradation. Similarly, the reaction kinetic model is included in Reference 16. Degradation at pH 4.3 and 7.4 are characterized in the previous work.[4] Scaffold degradation at pH 5.5 is characterized in this work. The final critical relaxation exponent is the average of all degradation experiments at a single pH.

μ^2rheology

Device fabrication

To enable the pH fluid environment to be consecutively changed, a previously designed two layer microfluidic device has been used. The details of device fabrication and theory of operation are reported in recent publications.[4,21–23] The device fabrication adapts the procedure developed by Schultz and Furst.[24–27]

Briefly, the channel design is first printed on a transparency (8.5 × 11 in, Apollo) with a black background and tha channel pattern is transparent. This is called the design negative. The stamp is made of UV curable thiolene resin (NOA 81, Norland Products, Inc.) on a piece of glass (75 × 50 × 1 mm, Fisher Scientific) using the design negative as a mask. UV light passes through the transparent channel design on the design negative and polymerizes the thiolene resin in the shape of the channels. The stamp then has the design of the channels polymerized onto it. Polydimethylsiloxane (PDMS, Sylgard 184, Dow Corning) is patterned over the stamps by curing overnight at 55°C. This creates channels in the PDMS. The patterned PDMS is cut and attached to a large glass coverslip (75 × 50 × 0.15 mm, Fisher Scientific) using oxygen plasma (Harrick Plasma).[28,29] This is the first layer of the device. The second layer, which is the solvent basin, is made of unpatterned PDMS that is cut into a circular chamber and sealed on top of the sample chamber using plasma treatment. A thin glass layer is synthesized inside the channel to prevent solvent uptake during long experiments. This is made by heating a pre-converted solution of tetraethoxysilane (Alfa Aesar), methyltriethoxysilane (Acros Organics), ethanol (Reagent Alcohol, Fisher Scintific) and pH 4.5 water adjusted by HCl (Ricca Chemical Company, LLC) at 100°C while the solution flows through the channels for 10 s.[21,30,31]

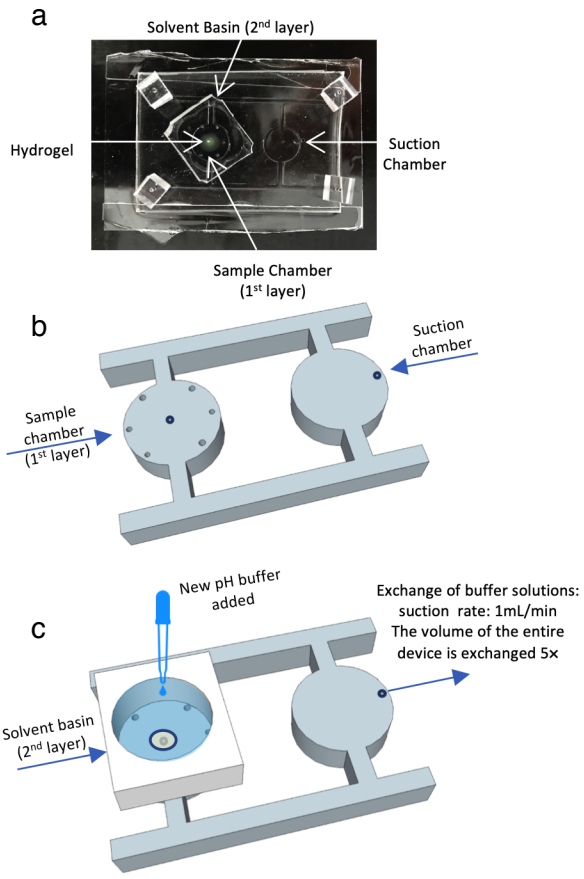

Figure S4: The microfluidic device used to mimic temporal pH changes in the GI tract. (a) An image of this two layer microfluidic device. Schematics of (b) the first layer of the device, with the sample chamber on the left and suction chamber on the right and (c) the second layer of the device including an illustration of buffer exchange. The CAH is injected into the sample chamber, which is below the solvent basin. The solvent basin connects to the sample chamber through six channels that are evenly distributed around the edge of the chamber. The fluid environment is exchanged by applying gentle suction in the suction chamber. Once suction is applied the new pH buffer enters the sample chamber through these six channels, generating equal pressure in the sample chamber that traps the CAH in place. This results in complete fluid exchange with minimal sample loss. Reproduced from Ref.[4] with permission from the Royal Society of Chemistry.

Device operation and μ^2rheology

Figure S4 shows this two layer design that enables multiple buffer exchanges with minimal sample loss. The bird's-eye view image of our microfluidic device is shown in Figure S4a, with a hydrazone CAH in the sample chamber. The first layer of device is composed of a sample chamber that is loaded with our sample and a suction chamber that enables buffer exchange, shown in Figure S4b. The second layer of the device is a solvent basin located on top of the sample chamber. The function of the solvent basin is to hold buffer solutions, illustrated in Figure S4c. There are six channels (0.15 mm diameter) designed and symmetrically spaced around the edge of the sample chamber, every 60°, which connect with the solvent basin. The incubation environment is changed in the sample chamber by applying gentle suction. This suction makes fluid flow from the solvent basin into the sample chamber through these six channels, creating equal pressure in the sample chamber. The equal pressure during fluid exchange traps the CAH in place resulting in fluid exchange with minimal loss of sample.

During μ^2rheology experiments, the first buffer solution is loaded into both layers of the device and then the hydrogel precursor solution is injected through the center channel of the sample chamber, enabling CAH incubation at this pH condition. Microrheological characterization is taken of static samples with no surrounding fluid flow. After measuring the degradation in the first pH buffer, the buffer is exchanged by continually adding new pH buffer (the pH that mimics the environment in the next part of the GI tract) to the solvent basin and applying gentle suction through the suction chamber. The suction pulls the new buffer into the sample chamber and removes the previous buffer. To ensure CAH degradation is measured at the new incubation pH, the entire volume of the device is exchanged $5\times$. This series of steps are repeated multiple times to mimic the transient pH changes in the entire GI tract.

Using μ^2rheology, CAH degradation is measured after temporal pH changes that mimic the pH in the GI tract. The data are collected every $6-10$ mins during the entire degradation time window. At each pH exchange, the device has been washed at least three times using

the new pH buffer to ensure degradation starts in the new pH environment. The buffer exchange takes around 15 mins and is not accounted for in the scaffold degradation time. After exchange, scaffold degradation is then characterized in the quiescent state using MPT. Throughout the μ^2rheology measurements there is no flow in the sample chamber, though the solvent basin is constantly refilled with buffer solution, preventing any effects from solvent evaporation.

Each μ^2rheology experiment of the entire GI tract is repeated at least 3 times, to ensure reproducibility of results.

Additional measurements of GI tract 1 and 2

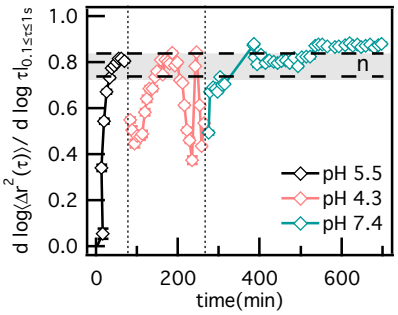

Figure S5: μ^2rheology measurements of temporal CAH degradation that mimics the pH environment in GI tract 1. The logarithmic slope of the MSD, $\alpha = \frac{d\log\langle\Delta r^2(\tau)\rangle}{d\log\tau}$, changes during scaffold degradation. The vertical dotted lines indicate buffer exchange, first from pH 5.5 to 4.3 then from pH 4.3 to 7.4. The horizontal dashed lines represent the bounds of the phase transition region defined by the critical relaxation exponent, n_{avg}. $n_{avg} = 0.79 \pm 0.05$ is determined using time-cure superposition.[4]

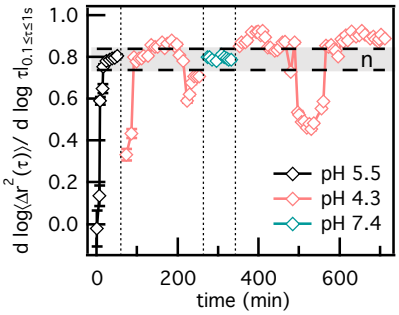

Figure S6: μ^2rheology measurements of consecutive degradation that mimics the pH in GI tract 2. The logarithmic slope of the MSD, $\alpha = \frac{d\log\langle\Delta r^2(\tau)\rangle}{d\log\tau}$, changes during degradation. The vertical dotted lines indicate buffer exchange. GI tract 2 has buffer exchanged from pH 5.5 to 4.3, from pH 4.3 to 7.4 and from pH 7.4 to 4.3. The horizontal dashed lines represent the upper and lower limits of the phase transition region, defined by the critical relaxation exponent, n_{avg}.[4]

Consecutive degradation with a single pH exchange

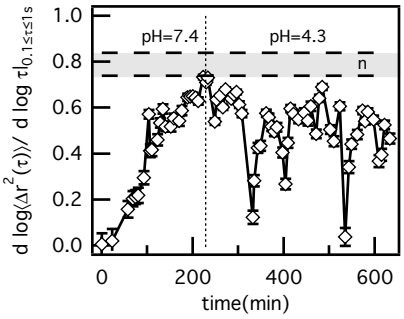

Figure S7: μ^2rheology measurements for CAH degradation at two different pHs, first at pH 7.4 then at pH 4.3. The logarithmic slope of the mean-squared displacement (MSD), $\alpha = \frac{d\log\langle\Delta r^2(\tau)\rangle}{d\log\tau}$, as a function of degradation time. The vertical dotted line shows when pH is exchanged from 7.4 to 4.3. The horizontal dashed lines are the bounds of the critical phase transition region determined using time-cure superposition.[4]

Comparison of degradation kinetics of two GI tracts

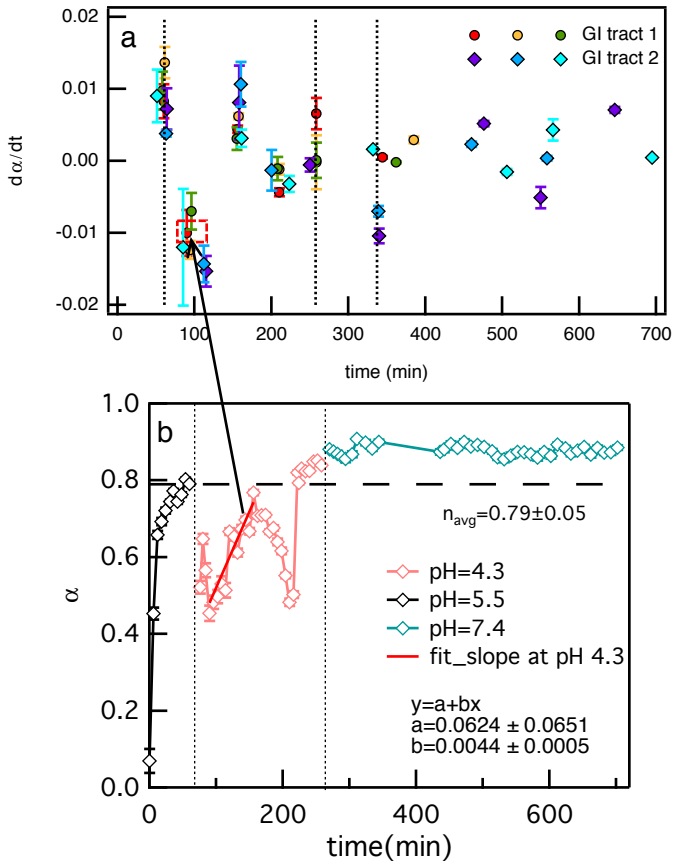

Figure S8: CAH degradation kinetics are compared at each pH from the two GI tracts. (a) The slopes calculated from the change in rheological properties over the same time intervals during either gelation or degradation in each experiment, $\frac{d\alpha}{dt}$, are plotted. Each tract is repeated three times, represented by different symbols. The vertical dotted lines represents the time when buffer is exchanged. (b) Using a portion of GI tract 1 as an example to illustrate the calculation of $\frac{d\alpha}{dt}$ during scaffold degradation. The arrow points out the slope, which is represented as the red dot in GI tract 1, and the data used to calculate $\frac{d\alpha}{dt}$. The error in (a) is the error in fitting the slope.

Table S1: The average rate of change of rheological properties, $\frac{d\alpha}{dt}$, and time of degradation-gelation cycles at pH 4.3 in each GI tract are calculated and listed in the table. The error in the rate values is propagated from the standard deviation of fitting each set of data. The error in the degradation-gelation cycles is the standard deviation in the time of each cycle. All values are from at least three replicates of each experiment in each GI tract scheme.

	GI tract 1	GI tract 2
pH 5.5 rate	0.0094 ± 0.0014	0.0067 ± 0.0013
pH 4.3 rate gelation	-0.0108 ± -0.0015	-0.0151 ± -0.0035
pH 4.3 rate degradation	0.0046 ± 0.0009	0.0067 ± 0.0022
pH 4.3 rate gelation	-0.0032 ± -0.0032	-0.0048 ± -0.0009
pH 4.3 cycle time (min)	132.67	128.33
pH 4.3 cycle time error (min)	11.02	35.02
pH 4.3 to pH 7.4 rate degradation	0.0024 ± 0.0006	0.0037 ± 0.0006
pH 4.3 rate gelation	N/A	-0.0023 ± -0.0013
pH 4.3 rate degradation	N/A	0.0043 ± 0.0008
pH 4.3 rate gelation	N/A	-0.0018 ± -0.0003
pH 4.3 cycle time (min)	N/A	100.67
pH 4.3 cycle time error (min)	N/A	44.56

References

(1) McKinnon, D. D.; Domaille, D. W.; Cha, J. N.; Anseth, K. S. Biophysically defined and cytocompatible covalently adaptable networks as viscoelastic 3D cell culture systems. *Advanced Materials* **2014**, *26*, 865–872.

(2) McKinnon, D.; Domaille, D.; Brown, T.; Kyburz, K.; Kiyotake, E.; Cha, J.; Anseth, K. Measuring cellular forces using bis-aliphatic hydrazone crosslinked stress-relaxing hydrogels. *Soft Matter* **2014**, *10*, 9230–9236.

(3) McKinnon, D. D.; Domaille, D. W.; Cha, J. N.; Anseth, K. S. Bis-aliphatic hydrazone-linked hydrogels form most rapidly at physiological pH: identifying the origin of hydrogel properties with small molecule kinetic studies. *Chemistry of Materials* **2014**, *26*, 2382–2387.

(4) Wu, N.; Schultz, K. M. Microrheological characterization of covalent adaptable hydrogels for applications in oral delivery. *Soft matter* **2019**, *15*, 5921–5932.

(5) Savin, T.; Doyle, P. S. Static and dynamic errors in particle tracking microrheology. *Biophysical journal* **2005**, *88*, 623–638.

(6) Crocker, J. C.; Grier, D. G. Methods of digital video microscopy for colloidal studies. *Journal of colloid and interface science* **1996**, *179*, 298–310.

(7) Valentine, M.; Perlman, Z.; Gardel, M.; Shin, J. H.; Matsudaira, P.; Mitchison, T.; Weitz, D. Colloid surface chemistry critically affects multiple particle tracking measurements of biomaterials. *Biophysical journal* **2004**, *86*, 4004–4014.

(8) Mason, T. G.; Weitz, D. Optical measurements of frequency-dependent linear viscoelastic moduli of complex fluids. *Physical review letters* **1995**, *74*, 1250.

(9) Mason, T. G. Estimating the viscoelastic moduli of complex fluids using the generalized Stokes–Einstein equation. *Rheologica Acta* **2000**, *39*, 371–378.

(10) Furst, E. M.; Squires, T. M. *Microrheology*; Oxford University Press, 2017.

(11) Winter, H. H.; Chambon, F. Analysis of linear viscoelasticity of a crosslinking polymer at the gel point. *Journal of rheology* **1986**, *30*, 367–382.

(12) Winter, H. Can the gel point of a cross-linking polymer be detected by the G′–G″ crossover? *Polymer Engineering & Science* **1987**, *27*, 1698–1702.

(13) Adolf, D.; Martin, J. E. Time-cure superposition during crosslinking. *Macromolecules* **1990**, *23*, 3700–3704.

(14) Chambon, F.; Winter, H. H. Linear viscoelasticity at the gel point of a crosslinking PDMS with imbalanced stoichiometry. *Journal of Rheology* **1987**, *31*, 683–697.

(15) Schultz, K. M.; Anseth, K. S. Monitoring degradation of matrix metalloproteinases-cleavable PEG hydrogels via multiple particle tracking microrheology. *Soft Matter* **2013**, *9*, 1570–1579.

(16) Escobar IV, F.; Anseth, K. S.; Schultz, K. M. Dynamic changes in material properties and degradation of poly (ethylene glycol)–hydrazone gels as a function of pH. *Macromolecules* **2017**, *50*, 7351–7360.

(17) Larsen, T. H.; Furst, E. M. Microrheology of the liquid-solid transition during gelation. *Physical review letters* **2008**, *100*, 146001.

(18) Wehrman, M. D.; Lindberg, S.; Schultz, K. M. Quantifying the dynamic transition of hydrogenated castor oil gels measured via multiple particle tracking microrheology. *Soft matter* **2016**, *12*, 6463–6472.

(19) Schultz, K. M.; Baldwin, A. D.; Kiick, K. L.; Furst, E. M. Gelation of Covalently Cross-Linked PEG- Heparin Hydrogels. *Macromolecules* **2009**, *42*, 5310–5316.

(20) Schultz, K. M.; Baldwin, A. D.; Kiick, K. L.; Furst, E. M. Measuring the modulus and reverse percolation transition of a degrading hydrogel. *ACS macro letters* **2012**, *1*, 706–708.

(21) Wehrman, M. D.; Milstrey, M. J.; Lindberg, S.; Schultz, K. M. Using μ 2 rheology to quantify rheological properties during repeated reversible phase transitions of soft matter. *Lab on a Chip* **2017**, *17*, 2085–2094.

(22) Wehrman, M. D.; Lindberg, S.; Schultz, K. M. Impact of shear on the structure and rheological properties of a hydrogenated castor oil colloidal gel during dynamic phase transitions. *Journal of Rheology* **2018**, *62*, 437–446.

(23) Wehrman, M.; Milstrey, M.; Lindberg, S.; Schultz, K. Combining Microfluidics and Microrheology to Determine Rheological Properties of Soft Matter during Repeated Phase Transitions. *Journal of visualized experiments: JoVE* **2018**,

(24) Schultz, K. M.; Furst, E. M. High-throughput rheology in a microfluidic device. *Lab on a Chip* **2011**, *11*, 3802–3809.

(25) Schultz, K. M.; Bayles, A. V.; Baldwin, A. D.; Kiick, K. L.; Furst, E. M. Rapid, high resolution screening of biomaterial hydrogelators by μ2rheology. *Biomacromolecules* **2011**, *12*, 4178–4182.

(26) Cabral, J. T.; Hudson, S. D.; Harrison, C.; Douglas, J. F. Frontal photopolymerization for microfluidic applications. *Langmuir* **2004**, *20*, 10020–10029.

(27) Harrison, C.; Cabral, J. T.; Stafford, C. M.; Karim, A.; Amis, E. J. A rapid prototyping technique for the fabrication of solvent-resistant structures. *Journal of Micromechanics and Microengineering* **2003**, *14*, 153.

(28) Ng, J. M.; Gitlin, I.; Stroock, A. D.; Whitesides, G. M. Components for integrated poly (dimethylsiloxane) microfluidic systems. *Electrophoresis* **2002**, *23*, 3461–3473.

(29) Whitesides, G. M.; Stroock, A. D., et al. Flexible methods for microfluidics. *Phys. Today* **2001**, *54*, 42–48.

(30) Abate, A. R.; Lee, D.; Do, T.; Holtze, C.; Weitz, D. A. Glass coating for PDMS microfluidic channels by sol–gel methods. *Lab on a Chip* **2008**, *8*, 516–518.

(31) Bhattacharya, S.; Datta, A.; Berg, J. M.; Gangopadhyay, S. Studies on surface wettability of poly (dimethyl) siloxane (PDMS) and glass under oxygen-plasma treatment and correlation with bond strength. *Journal of microelectromechanical systems* **2005**, *14*, 590–597.